

PSFC/JA-07-8

**Observation of the Decay Dynamics and  
Instabilities of Megagauss Field Structures  
in Laser- Produced Plasmas**

**C. K. Li, F. H. Séguin, J. A. Frenje, J. R. Rygg, and R. D. Petrasso**

*Plasma Science and Fusion Center, Massachusetts Institute of Technology,  
Cambridge, Massachusetts 02139, USA*

**R. P. J. Town, P. A. Amendt, S. P. Hatchett, O. L. Landen, A. J.  
Mackinnon, P. K. Patel, and M. Tabak**

*Lawrence Livermore National Laboratory, Livermore, California 94550 USA*

**J. P. Knauer, T. C. Sangster, and V. A. Smalyuk**

*Laboratory for Laser Energetics, University of Rochester, Rochester,  
New York 14623, USA*

14 May 2007

Plasma Science and Fusion Center  
Massachusetts Institute of Technology  
Cambridge, MA 02139 USA

The work described here was performed in part at the LLE National Laser User's Facility (NLUF), and was supported in part by US DOE (Grant No. DE-FG03-03SF22691), LLNL (subcontract Grant No. B504974), and LLE (subcontract Grant No. 412160-001G).

Accepted for publication in *Physical Review Letters*

# Observation of the Decay Dynamics and Instabilities of Megagauss Field Structures in Laser-Produced Plasmas

C. K. Li, F. H. Séguin, J. A. Frenje, J. R. Rygg, and R. D. Petrasso

*Plasma Science and Fusion Center, Massachusetts Institute of Technology, Cambridge, Massachusetts 02139, USA*

R. P. J. Town, P. A. Amendt, S. P. Hatchett, O. L. Landen, A. J. Mackinnon, P. K. Patel, and M. Tabak

*Lawrence Livermore National Laboratory, Livermore, California 94550 USA*

J. P. Knauer, T. C. Sangster, and V. A. Smalyuk

*Laboratory for Laser Energetics, University of Rochester, Rochester, New York 14623, USA*

Monoenergetic proton radiography was used to make the first measurements of the long-timescale dynamics and evolution of megagauss (MG) laser-plasma generated magnetic (B) field structures. While a 1-ns  $10^{14}$  W/cm<sup>2</sup> laser beam is on, the field structure expands in tandem with a hemispherical plasma bubble, maintaining a rigorous 2D cylindrical symmetry. With the laser off, the bubble continues to expand as the field decays; however the outer field structure becomes distinctly asymmetric, indicating instability. Similarly, localized asymmetry growth in the bubble interior indicates another kind of instability. 2D LASNEX hydro simulations qualitatively match the *cylindrically-averaged* post-laser plasma evolution but even then it underpredicts the field dissipation rate and of course completely misses the 3D asymmetry growth.

PACS numbers: 52.38 Fz, 52.50. Jm, 52.70. Nc

The long-term decay or relaxation of dynamical systems is of fundamental importance to diverse physical phenomena, be it a simple oscillator, spin-polarized [1] matter, or a solar flare [2]. Here we report, for the first time, on detailed observations and quantitative images of the decay of megagauss (MG) fields initially generated from a laser beam interacting with a foil. With the laser on and the system driven, the magnetic (B) field maintains, as it expands along the perimeter of a hemispherical plasma bubble, a rigorous degree of cylindrical symmetry [3]. However, when laser-drive ends, the B field structure continues to expand and decay but with clear 3 dimensional (3D), but distinctly different, structures emerging both along the edge and in the interior of the bubble. We hypothesize that these symmetry-breaking features, never before seen in any High-Energy-Density (HED) plasmas [4], are related to different instabilities [5-7] that arise during the decay phase.

In our experiments, monoenergetic 14.7-MeV proton radiography [3] was used to obtain gated images ( $\sim 150$  ps) of the field evolution during the laser-driven phase (0-1 ns) and, most importantly for this study, in the post-driven phase (1-3 ns). Because of the novelty of the isotropic, monoenergetic, pulsed source with matched detector, a precise field mapping, via the Lorentz force, is obtained for the duration, and over the entire physical expanse, of the expanding bubble. Using this same technique, we recently reported on the laser-driven phase of these dynamics whereby the field achieves  $\sim 0.5$  MG intensities [3]. Most other previous work in this field has involved much shorter laser pulses ( $\leq 10$  ps) [8] or  $\sim 1$  ns laser pulses but with limited diagnostic measurements [9] and has not resulted in the direct observation of any instabilities nor of any quantitative field maps at any time, let alone a sequence of them as presented here.

While the laser is on, the B field is generated primarily via  $\nabla n_e \times \nabla T_e$  [10] and is convected outward with the expanding bubble because the field is “frozen in.” After the laser turns off, the plasma begins to cool, becoming more collisional and increasingly resistive, thus allowing the field to diffuse relative to the fluid [10]. At these post-driven times, the fluid behavior near the bubble edge can be dominated by field and resistive effects, i.e. the plasma  $\beta$  (the ratio of thermal to field energy) can become smaller than one. This circumstance gives rise to the possibility of resistive instabilities.

The setup of the experiments, performed at the OMEGA laser facility [11], is illustrated schematically in Fig. 1. B fields were generated through laser-plasma interactions on a plastic (CH) foil by a single laser beam (henceforth called the *interaction beam*) with a wavelength of 0.351  $\mu\text{m}$ , linearly polarized, and incident at  $23^\circ$  from the normal direction. The 1-ns-long square laser pulse had an energy of  $\sim 500$ J and a spot diameter of 800 $\mu\text{m}$  determined by phase plate SG4 (defined as 95% energy deposition) [12], resulting in a laser intensity of order  $10^{14}$  W/cm<sup>2</sup>.

The fields were studied with monoenergetic proton radiography using a backlighter that produced protons

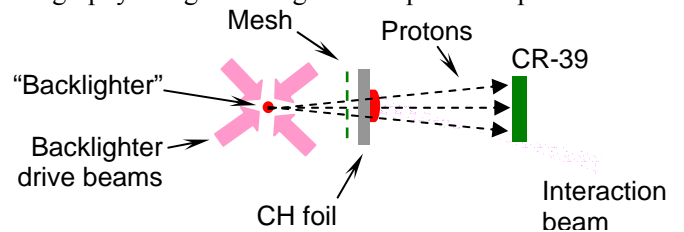


FIG. 1 (Color online) Schematic illustration of the experiment setup for face-on proton radiography. Distances from the backlighter are 1.3 cm for the mesh, 1.5 cm for the CH foil (5  $\mu\text{m}$  thick), and 30 cm for the CR-39 detector.

isotropically at the discrete energy of 14.7 MeV (fusion products of the nuclear reaction  $D+{}^3\text{He}\rightarrow\alpha+p$ , generated from  $D^3\text{He}$ -filled, exploding-pusher implosions driven by 20 OMEGA laser beams) [3]. A nickel mesh (60  $\mu\text{m}$  thick with a 150- $\mu\text{m}$  hole-to-hole spacing and 75- $\mu\text{m}$  holes) was used to divide the backlighter protons into discrete beamlets before they passed through the foil, and radiographs were recorded using CR-39 detectors [13]. The duration of each “exposure”, determined by the length of time the backlighter produced protons, was  $\sim 150$  ps. Since the backlighter-to-foil flight time for the protons was  $\sim 0.28$  ns, an image representing the state of the field at the foil at time  $t_a$  after the onset of the interaction beam was made by starting this beam a time  $t_a + 0.28$  ns after the mean backlighter production time.

To aid in interpretation of these observations, simulations [14] with the 2D hydrodynamic code LASNEX [15] and hybrid PIC code LSP [16] were also performed. In addition these observations comprise stringent new tests of LASNEX in ways that have hitherto been unavailable and, as we will see, significant differences do arise between observations and simulations during the post-driven phase.

Face-on images are shown in Fig. 2 (a). Each image is labeled with a time that represents the interval between the start of the interaction beam and the arrival of the backlighter protons, and shows how the proton beamlets were deflected while passing through the B field that formed around the bubble, as described previously [3]. For times when the interaction beam was on, each image has a sharp circular ring where beamlets pile up after passing through the edges of the bubble where the B fields were largest (see Fig. 3). This circle is a magnified image of the bubble edge, because the angular deflection of each beamlet is proportional to  $\int \mathbf{B}\times d\mathbf{l}$  (where  $d\mathbf{l}$  is the

differential pathlength along the proton trajectory) and  $\mathbf{B}\times d\mathbf{l}$  points away from the bubble center. Angular deflection of a beamlet at the bubble results in lateral displacement of the beamlet at the detector plane by a vector  $\xi$  ( $\propto \int \mathbf{B}\times d\mathbf{l}$ ) relative to where the beamlet would have been detected in the absence of a field. Beamlets in the center of each image undergo less deflection, indicating that  $\int \mathbf{B}\times d\mathbf{l}$  is smaller there. These features are reasonably well reproduced by LASNEX+LSP simulations, as shown in Fig. 2b for 0.3 to 0.9 ns. Figure 3a shows the B field predicted in these simulations in a plane perpendicular to the foil at 0.6 ns. The protons would travel from left to right in the plane of this field map, and the maximum angular deflections would be for trajectories passing through the bubble edges.

After the interaction laser ends, the simulations continue to generally track the behavior of the real data, though less well. The simulations indicate the presence of two rings, the outer one due to the expanding bubble surface, the inner due to fields at the edge of the hole burned through the plastic by the laser, as shown in Fig. 2 between 1.5 and 3.0 ns. The data also have these two rings, but the one representing the outer bubble boundary becomes strikingly asymmetric, with 5 to 10 cycles over the circumference. In addition, the beamlet displacements in the data are much smaller than those in the simulation, indicating that fields have diminished much more quickly than predicted (though both simulation and experiment show a continued expansion of the plasma bubble at late times, leading to convective field dissipation).

These effects can be quantified by measuring the sizes of features in the images and the displacements  $\xi$  of individual beamlets seen in the images, because for our truly monoenergetic backlighter there is an exact and unambiguous proportionality between  $\xi$  and  $\int \mathbf{B}\times d\mathbf{l}$ . The

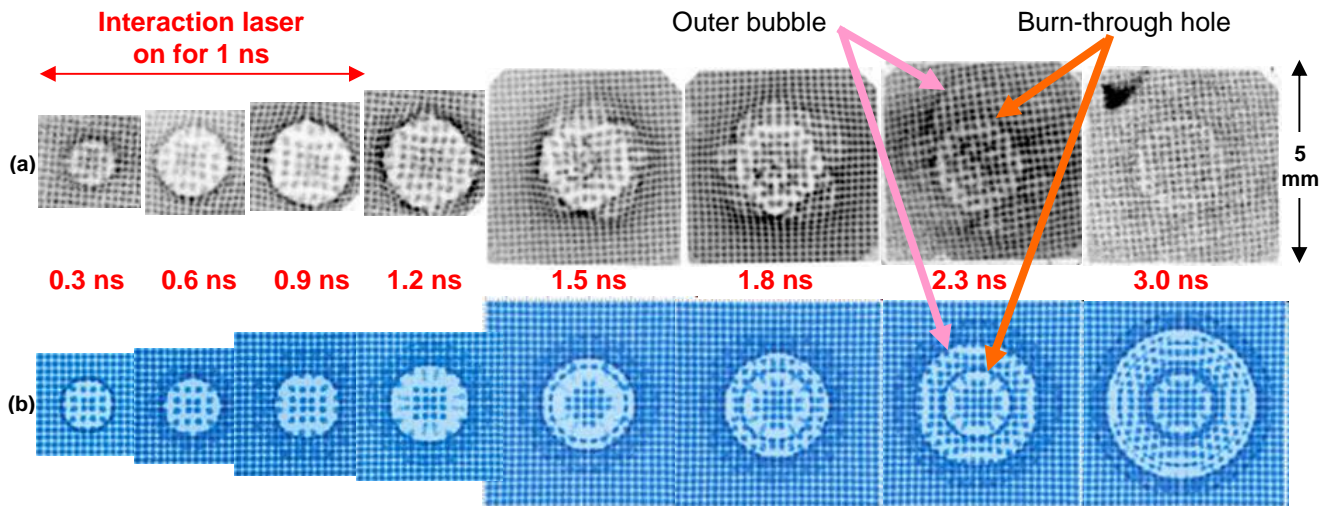


FIG. 2 (Color) (a) Measured face-on  $D^3\text{He}$  proton images showing the spatial structure and temporal evolution of B fields generated by laser-plasma interactions. Each image is labeled by the time between the arrival at the foil of the interaction beam and the arrival of the imaging protons. The images illustrate the transition from the 1-ns illumination period, with 2D symmetric expansion of B fields, to a post-laser decay phase with 3D structures emerging around the bubble edge and in the interior while the expanding bubble cools and becomes increasingly resistive. (b) Corresponding images simulated by LASNEX+LSP. Arrows point to the image features corresponding to fields at the outer bubble boundary and at the laser burn-through hole shown in Fig. 3b.

actual bubble size is not the apparent size in the image, because of the magnification referred to above. The true position of the bubble edge is determined by the locations the beamlets in the pileup region would have had in the image if they weren't displaced. Sizes determined in this manner are shown in Fig. 4a, where the radius at late times when the bubble is asymmetric represents an angular average. The bubble radius grows linearly while the laser is on, and then continues to expand after the laser is off. The burn-through hole radius is also shown in Fig. 4a. The agreement between data and simulation is, in this averaged sense, quite good for both radii at all times. The amplitudes of the measured asymmetries in the outer bubbles in Fig. 2a are plotted in Fig. 4b. Shown in Fig. 4c, the peak value occurs at the end of the laser pulse, and it decays thereafter. We note that while the laser is on this maximum occurs at the outside of the bubble, but after the laser is off the maximum occurs at the edge of the burn-through hole in both data and simulation. The maximum amplitude agrees well for data and simulation, but the data fall off faster than the simulations; this suggests that the actual  $T_e$  drops more quickly than in the simulation, enhancing the resistivity and allowing the fields to diffuse and dissipate more quickly.

The net result of the data-simulation comparison is that the 2D code does a reasonable job of predicting the cylindrically “averaged” 2D behavior of the bubble and B field generation and expansion, but underestimates the rate of field dissipation and of course doesn't predict the 3D structure of the asymmetry seen in the data. It might be argued that our observation of 3D structure renders

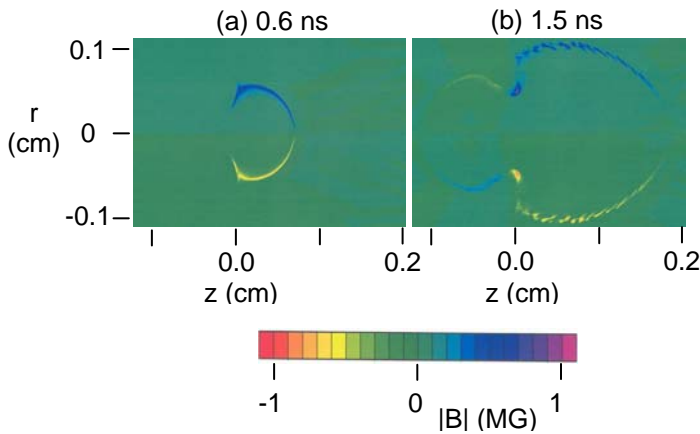


FIG. 3 (Color) LASNEX-simulated B field strength on cross sections of the bubble in a plane perpendicular to the foil at (a)  $\sim 0.6$  ns, when laser was on, and (b)  $\sim 1.5$  ns, when laser was off. The horizontal coordinate  $z$  is distance from the foil (the laser is incident from the right and the proton from the left) and the vertical coordinate  $r$  is distance from the central axis of the plasma bubble. When the laser is on, strong fields occur near the edge of the bubble. After the laser pulse, strong fields also appear near the edge of the hole burned into the foil by the laser; they generate the inner circle seen in Fig. 2 for times 1.5 ns and later. The simulations also predict a second bubble on the rear of the foil after burnthrough; but the simulated images show no feature associated with the field there because it is relatively weak.

comparison with the 2D simulations irrelevant, but 3D codes are not yet available and it is important to know what can and cannot be predicted with the tools at hand. (Work is currently underway on combining the 3D hydro code HYDRA with a field generating package [17].) Experimental measurements such as those shown here are important because they directly reveal previously unpredicted physical phenomena, they indicate the fundamental importance of 3D processes in certain regimes, such as in this decay phase, and they provide invaluable information for benchmarking true 3D code development in the future.

We do not have a complete model for the instability behind the observed periodicity and growth rate of the asymmetry, but the observation itself is new and important. Strong image-to-image similarities in the angular structure of the asymmetry, in spite of the fact that the images are from different shots, must be connected with some constant physical characteristic of the experiment, but the foil has no directional characteristics and the mesh has structure but, in the experiments reported here, is too far (2 mm) behind the foil to be responsible. Furthermore, even changing the mesh

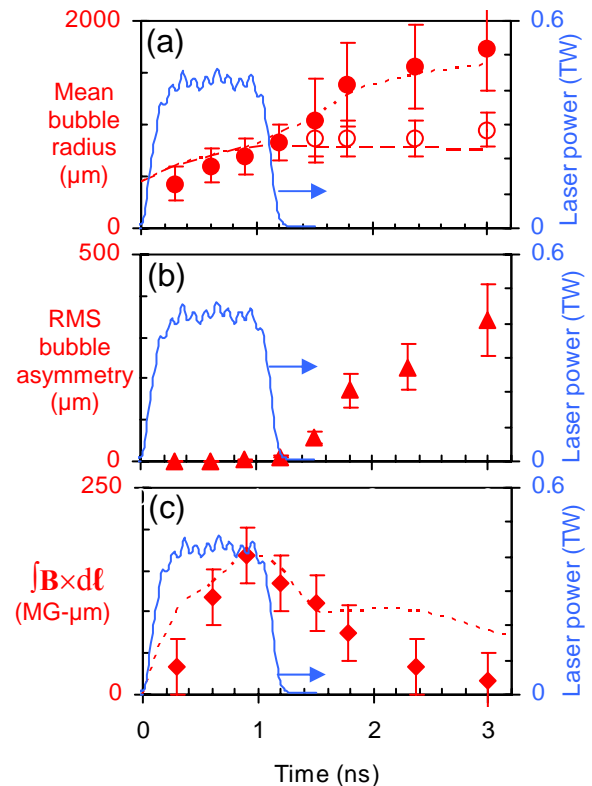


FIG. 4 (Color online) (a) Evolution of sizes at the foil of the bubble (solid circles) and the burn-through hole (open circles), compared with 2D LASNEX+LSP simulations (dashed lines), inferred from the images of Fig. 2. Because of the emerging 3D asymmetries, the data points represent averages over azimuthal angle. The blue line shows the 1-ns OMEGA laser pulse. (b) RMS deviations of the outer bubble boundary from the average radii shown in (a), as a function of time (this is zero in the simulations). (c) Evolution of the maximum measured value of  $|\int \mathbf{B} \times d\mathbf{l}|$  (diamonds), compared with simulations (dashed line).

distance from 2 mm to 0.125 mm had no effect on the growth or amplitude of this instability, nor did the effects changing the laser from polarized to unpolarized light.

This is the first observation of such an instability in laser-produced HED plasmas. It is plausible that this is a pressure-driven, resistive Magnetohydrodynamic (MHD) interchange instability [6], resulting in an interchange of field between the inside and outside of the bubble surface. It occurs under circumstances such as we have here, with unfavorable field curvature ( $\boldsymbol{\kappa} \cdot \nabla p > 0$ , where  $\boldsymbol{\kappa} = \mathbf{B} \cdot \nabla \mathbf{B} / B^2$  is the field-line curvature and  $\nabla p$  is the pressure gradient) and when resistivity allows for radial diffusion of B field into the region outside the bubble. It makes sense that this instability would occur only after the laser is off, as shown in Fig. 4b, when the cooling plasma becomes more resistive. Of course, we cannot, without additional experiments, completely rule out the possible role of other MHD instabilities, such as kink or tearing modes [6], but they seem less likely to have the observed spatial configuration. Pure fluid instabilities such as the Widnall type [18], on the other hand, might be expected to be visible while the laser is on (when B fields don't have much impact on the flow but are frozen in); but we don't see any evidence for the instability then.

Another type of instability is apparent during the interval from 1.5 to 2.3 ns, where the distributions of beamlets near the image centers have some chaotic structure. Since the structure is different in each of the three images (which are from different shots), it appears that the structure is random. We noted in earlier work [3] that qualitatively similar chaotic structures occur while the laser is on only if laser phase plates were not used; the phase plates either prevented the chaotic structure from forming as long as the laser was on, or reduced its amplitude sufficiently that it was not visible until it had a chance to grow over a longer time period. In the case at hand, we conjecture that, as the plasma cools and becomes increasingly resistive, an electron thermal instability is triggered and, driven by the heat flow, leads to random filamentary structure of  $n_e$  and  $T_e$ , as well as B fields [19]. Such instability occurs only in the center region where the mean free path,  $\lambda_{mfp}$ , is smaller than the electron collisionless skin depth  $c\omega_{pe}^{-1}$ , i.e.  $\lambda_{mfp}/c\omega_{pe}^{-1} \sim (\omega_{ce}\tau L_{\parallel}/L_{\perp})^{1/2} < 1$ , where  $\omega_{ce}\tau$  is the Hall parameter,  $L_{\parallel}$  and  $L_{\perp}$  are parallel and perpendicular scale lengths, respectively.

In summary, using monoenergetic proton radiography, we have measured the long-timescale dynamics and evolution of the spatial and temporal structure of MG fields, with unprecedented detail and accuracy, generated by laser-plasma interactions. Importantly, the first observations were obtained of asymmetric instabilities that occurred in the post-driven phase after the interaction laser ends, at which time the resistivity increased, due to plasma cooling, at a rate faster than predicted by 2D LASNEX simulations. Interestingly, these instabilities broke the 2-D symmetry that rigorously prevailed through

out the laser drive. The observations demonstrate that 2D simulations are intrinsically unable to model the evolution of the fields during post-driven period thus stimulating the need for 3-D hydro capabilities that include field generating capabilities [17]. Finally, these observations have provided new insights, hitherto unavailable, into the behavior and stability and decay of laser-produced plasmas and fields. They potentially open new areas of research in HED physics, including monoenergetic particle probing of warm dense matter and the backlighting of implosions and laboratory astrophysical experiments with the aim of characterizing areal density and fields, such as might occur, in the latter case, at shock-front interfaces.

The work described here was performed in part at the LLE National Laser User's Facility (NLUF), and was supported in part by US DOE (Grant No. DE-FG03-03SF22691), LLNL (subcontract Grant No. B504974), and LLE (subcontract Grant No. 412160-001G).

- 
- [1] P. Herczeg *et al.*, *Physics Beyond the Standard Model* (World Scientific, Singapore, 1999).
  - [2] W. Baumjohann and R. A. Treumann, *Basic Space Plasma Physics* (Imperial College Press, London 1996).
  - [3] C. K. Li *et al.*, *Phys. Rev. Lett.* **97**, 135003 (2006).
  - [4] R. C. Davidson, *Frontiers in High Energy Density Physics* (National Academies Press, Washington 2003).
  - [5] B. B. Kadomtsev, *Review of Plasma Physics* (Consultants Bureau, New York, 1966).
  - [6] J. P. Freidberg, *Ideal Magnetohydrodynamics* (Plenum Press, New York 1987).
  - [7] M. G. Haines, *Phys. Rev. Lett.* **78**, 254 (1997).
  - [8] J. A. Stamper *et al.*, *Phys. Rev. Lett.* **26**, 1012 (1971); D. G. Colombant *et al.*, *ibid* **38**, 697 (1977); M. Borghesi *et al.*, *ibid* **81**, 112 (1998); A. J. Mackinnon *et al.*, *Rev. Sci. Instrum.* **75**, 3531 (2004).
  - [9] M. G. Drouet *et al.*, *Phys. Rev. Lett.* **36**, 591 (1976); M. A. Yates *et al.*, *ibid* **49**, 1702
  - [10] S. Eliezer, *The Interaction of High-Power Lasers with Plasmas* (IOP Pub. Bristol, 2002).
  - [11] T. R. Boehly *et al.*, *Opt. Commun.* **133** 495 (1997).
  - [12] T. J. Kessler *et al.*, *Laser coherence control: technology and applications* (SPIE, Bellingham WA 1993).
  - [13] F. H. Séguin *et al.*, *Rev. Sci. Instrum.* **75**, 3520 (2004).
  - [14] R. P. J. Town *et al.*, *Bull. Am. Phys. Soc.* **51**, 142 (2006).
  - [15] G. B. Zimmerman and W. L. Kruer, *Comm. in Plas. Phys. and Contr. Fus.* **2**, 51 (1975).
  - [16] D. R. Welch *et al.*, *Nucl. Inst. Meth. Phys. Res. A* **464**, 134 (2001).
  - [17] J. Koning *et al.*, *Bull. Am. Phys. Soc.* **51**, 167 (2006); M. M. Marinak, private communication (2007).
  - [18] S. E. Widnall *et al.*, *J. Fluid Mech.* **66**, 35 (1974).
  - [19] M. G. Haines, *Phys. Rev. Lett.* **47**, 917 (1981).